Chemical Engineering Journal 316 (2017) 82–90

Contents lists available at ScienceDirect

Chemical Engineering Journal

journal homepage: www.elsevier.com/locate/cej

Perchlorate, nitrate, and sulfate reduction in hydrogen-based membrane biofilm reactor: Model-based evaluation

Xueming Chen [a], Yiwen Liu [b], Lai Peng [c], Bing-Jie Ni [a,*]

[a] Advanced Water Management Centre, The University of Queensland, St. Lucia, Brisbane, QLD 4072, Australia
[b] Centre for Technology in Water and Wastewater, School of Civil and Environmental Engineering, University of Technology Sydney, Sydney, NSW 2007, Australia
[c] Laboratory of Microbial Ecology and Technology (LabMET), Ghent University, Coupure Links 653, 9000 Ghent, Belgium

HIGHLIGHTS

- A model was developed to describe ClO_4^-, NO_3^-, and SO_4^{2-} reduction in H_2-based MBfR.
- Two sensitive kinetic parameters were estimated using experimental data.
- MBfR performance and microbial structure were assessed under different conditions.
- SO_4^{2-} reduction could be restricted through proper control over the H_2-based MBfR.

GRAPHICAL ABSTRACT

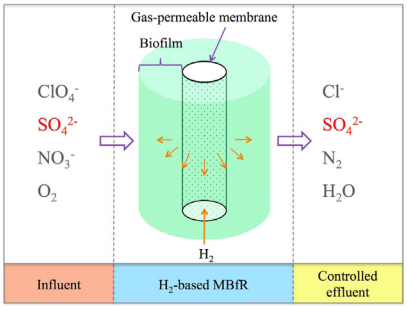

ARTICLE INFO

Article history:
Received 10 December 2016
Received in revised form 19 January 2017
Accepted 20 January 2017
Available online 22 January 2017

Keywords:
Hydrogen-based membrane biofilm reactor
Perchlorate
Nitrate
Sulfate
Mathematical modeling

ABSTRACT

A biofilm model was developed to evaluate the key mechanisms including microbially-mediated ClO_4^-, NO_3^-, and SO_4^{2-} reduction in the H_2-based membrane biofilm reactor (MBfR). Sensitivity analysis indicated that the maximum growth rate of H_2-based denitrification (μ_1) and maximum growth rate of H_2-based SO_4^{2-} reduction (μ_3) could be reliably estimated by fitting the model predictions to the experimental measurements. The model was first calibrated using the experimental data of a single-stage H_2-based MBfR fed with different combinations of ClO_4^-, NO_3^-, and/or SO_4^{2-} together with a constant dissolved oxygen (DO) concentration at three operating stages. μ_1 and μ_3 were determined at 0.133 h^{-1} and 0.0062 h^{-1}, respectively, with a good level of identifiability. The model and the parameter values were further validated based on the experimental data of a two-stage H_2-based MBfR system fed with ClO_4^-, NO_3^-, SO_4^{2-}, and DO simultaneously but at different feeding rates during two running phases. The validated model was then applied to evaluate the quantitative and systematic effects of key operating conditions on the reduction of ClO_4^-, NO_3^-, and SO_4^{2-} as well as the steady-state microbial structure in the biofilm of a single-stage H_2-based MBfR. The results showed that i) a higher influent ClO_4^- concentration led to a higher ClO_4^- removal efficiency, compensated by a slightly decreasing SO_4^{2-} removal; ii) the H_2 loading should be properly managed at certain critical level to maximize the ClO_4^- and NO_3^- removal while limiting the growth of sulfate reducing bacteria which would occur in the case of excessive H_2 supply; and iii) a moderate hydraulic retention time and a relatively thin biofilm were required to maintain high-level removal of ClO_4^- and NO_3^- but restrict the SO_4^{2-} reduction.

* Corresponding author.
E-mail address: b.ni@uq.edu.au (B.-J. Ni).

http://dx.doi.org/10.1016/j.cej.2017.01.084
1385-8947/

Nomenclature

MBfR	membrane biofilm reactor
μ_1	maximum growth rate of H_2-based denitrification (h^{-1})
μ_2	maximum growth rate in H_2-based ClO_4^- reduction (h^{-1})
μ_3	maximum growth rate of H_2-based SO_4^{2-} reduction (h^{-1})
DO	dissolved oxygen
MCL	maximum contamination level
PRB	perchlorate reducing bacteria
HDB	H_2-based denitrifying bacteria
SRB	sulfate reducing bacteria
HB	heterotrophic bacteria
SOB	sulfide oxidizing bacteria
UAP	utilization-associated products
BAP	biomass-associated products
SMP	soluble microbial products
EPS	extracellular polymeric substances
L_{H2}	H_2 surface loading (g COD m^{-2} h^{-1})
HRT	hydraulic retention time (h)
L_f	biofilm thickness (μm)
Y	yield coefficient of biomass growth
Y_0	yield of growth on H_2 and O_2 (g COD g^{-1} COD)
L	H_2 flux (g m^{-2} d^{-1})
S_g	H_2 concentration in the gas compartment (g m^{-3})
S_l	H_2 concentration in the biofilm matrix compartment (g m^{-3})
k	overall mass transfer coefficient (m d^{-1})
H	Henry coefficient (mol m^{-3} gas/mol m^{-3} liquid)

1. Introduction

Perchlorate (ClO_4^-) and nitrate (NO_3^-) are contaminants commonly present in surface water and groundwater. ClO_4^- is a byproduct of the production of rocket fuels and fireworks [1,2] and can cause severe health problems through interfering with the thyroid hormone production [3]. The ClO_4^- concentration in groundwater is typically below 100 μg L^{-1} but could reach 20 mg L^{-1} or more [4]. Though the maximum contamination level (MCL) for ClO_4^- hasn't been established by the US EPA, cleanup levels in drinking water ranging from 2 to 18 μg L^{-1} for ClO_4^- have been adopted by some states in the US [5]. NO_3^- usually co-occurs with ClO_4^- in groundwater and can lead to methemoglobinemia in infants [6]. Currently, the NO_3^- contamination level in the US and some European countries has been reported to reach up to 200 mg L^{-1} [7]. The MCL for NO_3^- is set/recommended at 11.3 mg N L^{-1} by European Union countries and the WHO [8], while it's been documented at 10 mg N L^{-1} by the US EPA.

To achieve simultaneous ClO_4^- and NO_3^- removal, biological processes are preferred due to their advantages over physical-chemical methods in terms of treatment costs. The H_2-based membrane biofilm reactor (MBfR) has been proved to be capable of driving the respiratory reduction of various oxidized contaminants, including ClO_4^-, NO_3^-, sulfate (SO_4^{2-}), selenate (SeO_4^{2-}), chromate (CrO_4^{2-}), bromate (BrO_3^-), and trichloroethene [9–14]. For example, Zhao et al. [9] proposed the usage of a H_2-based MBfR for the concurrent reduction of ClO_4^- and NO_3^-. In such an MBfR, ClO_4^- and NO_3^- were provided in the bulk liquid while H_2 as the electron donor was delivered through gas-permeable membranes. This counter-diffusional supply of gas and liquid substrates conduced to the rapid oxidation of H_2 in the biofilm, ensuring high-level utilization of H_2 and hence negligible loss to the atmosphere or effluent. Functional microorganisms including perchlorate reducing bacteria (PRB) and H_2-based denitrifying bacteria (HDB) attached naturally onto the membrane outer surface and formed a condensed and stable biofilm. As H_2 served as the mutual electron donor for both PRB and HDB, NO_3^- was found to inhibit ClO_4^- reduction due to microbial competitions under the condition of limited H_2 [9]. This inhibitory effect was greatly alleviated when sufficient H_2 was available [15].

SO_4^{2-} serves as another oxidized electron acceptor which frequently occurs together with ClO_4^- and NO_3^- [16]. Different from ClO_4^- and NO_3^-, the presence of SO_4^{2-} is generally not considered as a serious health concern. However, SO_4^{2-} reduction is an undesirable process due to its production of sulfide, which is not only malodorous and corrosive [17] but also toxic to human as well as a variety of microorganisms [18]. Therefore, SO_4^{2-} reduction should be minimized when treating water polluted with ClO_4^-, NO_3^-, and SO_4^{2-} simultaneously. Zhao et al. [16] applied a two-stage H_2-based MBfR system to study complete ClO_4^- reduction in the presence of NO_3^- and SO_4^{2-}. Albeit complete ClO_4^- and NO_3^- reduction could be obtained in the effluent, a lead MBfR needed to be implemented to provide a suitable feed for the lag MBfR. In addition, reoxygenation was applied to the effluent of the lead MBfR before it entered the lag MBfR to suppress SO_4^{2-} reduction. Another study by Zhao et al. [19] investigated the interactions among multiple electron acceptors (i.e., ClO_4^-, NO_3^-, and SO_4^{2-}) in a single-stage H_2-based MBfR. Despite the high-level (close to 100%) simultaneous removal of ClO_4^- and NO_3^-, a considerable SO_4^{2-} reduction (~60%) was observed. In brief, challenge still remains in achieving complete ClO_4^- and NO_3^- removal without incurring SO_4^{2-} reduction in the single-stage H_2-based MBfR.

Therefore, more efforts linking the operating conditions to the microbial community structure as well as the system performance of the single-stage H_2-based MBfR should be devoted to enforcing simultaneous removal of ClO_4^- and NO_3^- while eliminating SO_4^{2-} reduction. A multi-species biofilm model is of particular interest for qualitatively as well as quantitatively assessing such a single-stage H_2-based MBfR with multiple bacterial species, feeding substrates, and acting mechanisms involved. Therefore in this work, a biofilm model integrating the key mechanisms including microbially-mediated ClO_4^-, NO_3^-, and SO_4^{2-} reduction in the H_2-based MBfR was developed through expanding the previously established models [20–22] by taking into account the new roles of sulfur cycle from sulfide back to sulfate and the key effects of dissolved oxygen (DO) which is commonly present in groundwater on the H_2-based MBfR. The model was calibrated using the operational data of the single-stage H_2-based MBfR reported in Zhao et al. [19], which was fed with different combinations of ClO_4^-, NO_3^-, and/or SO_4^{2-} together with a constant DO concentration at three operating stages. The model was further validated based on the reported experimental data of the two-stage H_2-based MBfR system [16], fed with ClO_4^-, NO_3^-, SO_4^{2-}, and DO simultaneously but at different feeding rates during two running phases. The model was then applied to evaluate the quantitative and systematic effects of key operating conditions such as influent ClO_4^- concentration, H_2 surface loading (L_{H2}), hydraulic retention time (HRT), and biofilm thickness (L_f) on the reduction of ClO_4^-, NO_3^-, and SO_4^{2-} as well as the steady-state microbial community structure of the single-stage H_2-based MBfR fed with ClO_4^-, NO_3^-, SO_4^{2-}, and DO simultaneously. The related H_2 utilization of the MBfR was also assessed from the economic point of view.

2. Materials and methods

2.1. Model development

The multi-species model in this work was developed through expanding the biofilm model for simultaneous ClO_4^- and NO_3^- reduction [20,21] and the biofilm model for simultaneous NO_3^- and SO_4^{2-} reduction [22]. Related information such as biofilm density and diffusive properties and the anoxic mechanisms of HDB, PRB, sulfate reducing bacteria (SRB), and heterotrophic bacteria (HB) were directly adopted therefrom. In brief, H_2 served as the electron donor and energy source driving the microbial reduction of ClO_4^-, NO_3^-, and SO_4^{2-}. The energy gained from these redox reactions allowed synthesis of new biomass. Electrons were fractionized in light of mass balance for the accompanying production of utilization-associated products (UAP) and extracellular polymeric substances (EPS). Hydrolysis converted EPS to biomass-associated products (BAP), which together with UAP were oxidized by HB to reduce NO_3^-. Yield coefficient (Y) was generally used to link biomass growth and UAP and EPS formation to substrate consumption. On top of that, the sulfur cycle from S^{2-} back to SO_4^{2-} by sulfide oxidizing bacteria (SOB) and the role of oxygen which necessitates aerobic mechanisms of microorganisms involved were also considered in the model. It has to been noted that UAP and BAP are lumped into soluble microbial products (SMP) in the model. This simplification is well justified by the same values of parameters applied in Tang et al. [20,22] to describe the kinetics of heterotrophic growth on UAP and BAP. In total, the model describes the relationships among seven dissolved components, i.e., hydrogen (S_{H2}), nitrate (S_{NO3}), perchlorate (S_{ClO4}), sulfate (S_{SO4}), oxygen (S_{O2}), sulfide (S_S), and SMP (S_{SMP}), and seven particulate components, i.e., HDB (X_{HDB}), PRB (X_{PRB}), SRB (X_{SRB}), SOB (X_{SOB}), HB (X_{HB}), inert organics (X_I), and EPS (X_{EPS}), as detailed in Table S1 in the Supporting Information (SI). Aerobic growth was included in addition to anoxic growth for all the microorganisms in the model, with incorporation of non-competitive oxygen inhibition functions into the corresponding kinetic rate expressions. Dual-substrate Monod equations were applied to describe the species-specific interactions between electron acceptors (ClO_4^-, NO_3^-, SO_4^{2-}, and O_2) and electron donors (H_2, S^{2-}, and SMP). Similar to Tang et al. [22], SRB were assumed to use H_2 as the sole electron donor in the model, in view of the much higher growth rate of SRB on H_2 than SMP. Consistent with Tang et al. [20], PRB were assumed to be capable of respiring on both ClO_4^- and NO_3^- under anoxic H_2-reducing conditions. Referring to Tang et al. [20,22], the intermediate NO_2^- was not specifically included in the model considering its higher H_2-utilization priority as compared to ClO_4^- and SO_4^{2-} as well as the fact that NO_2^- was not detected in related H_2-based MBfR systems. Tables S2 and S3 in the SI summarize the stoichiometrics and kinetics of the developed model. The definitions, values, units, and sources of all parameters used in the developed model are listed in Table S4 in the SI.

The one-dimensional biofilm model was then constructed to simulate the bioconversion processes as well as the microbial community structure for the H_2-based MBfR through employing the software AQUASIM 2.1d [23]. The MBfR was modeled to be composed of a completely mixed gas compartment which represents the membrane lumen and a biofilm compartment which contains the biofilm and bulk liquid. The H_2 supply to the biofilm was simulated using a diffusive link connecting the gas compartment to the base of the biofilm. The specifications as well as the influent conditions in the model were set according to the conditions of experiments, the data of which were used for the subsequent model evaluation. Same as Tang et al. [20], all dissolved components at the biofilm's outer surface were subject to a consistent-flux boundary condition; a dissolved-component flux through the diffusion layer equalled the flux of this dissolved component in or out of the biofilm. The transport of dissolved components through the diffusion layer and into or out of the biofilm was described with the resistance approach using Fick's first law. The H_2 flux L from the gas compartment to the biofilm compartment through the membrane was modelled using the following equation [24,25] and implemented in AQUASIM through defining the diffusive link. Diffusion coefficients for dissolved components in the biofilm liquid phase were set at 0.8-fold of the values in water. More details related to the biofilm model setup can be found in Chen et al. [26].

$$L = k\left(\frac{S_g}{H} - S_l\right) \quad (1)$$

where S_g and S_l are the H_2 concentrations in the gas and biofilm matrix compartments (g m^{-3}), respectively, k is the overall mass transfer coefficient (m d^{-1}), and H is the Henry coefficient (mol m^{-3} gas/mol m^{-3} liquid).

2.2. Experimental data testing the developed model

Experimental data from the single-stage H_2-based MBfR reported in Zhao et al. [19] were used to calibrate the developed model. The single-stage MBfR contained a bundle of 32 composite hollow fiber membranes fixed at the bottom and another bundle of 10 hollow fiber membranes in a separate tube which were used for microbial community analysis. The liquid was continuously recirculated through a peristaltic pump at 100 mL min^{-1}. The influent feeding was maintained at 0.25 mL min^{-1}, the H_2 pressure at 5 psig, and the temperature at 25 °C for all tests. The MBfR was initially inoculated with diluted activated sludge obtained from a wastewater treatment plant, and the microbial community was enriched by circulating 10 g m^{-3} ClO_4^- for 24 h. Once the enrichment was obtained, three-stage tests with different combinations of ClO_4^-, NO_3^-, and/or SO_4^{2-} were conducted with the MBfR: ClO_4^- at Stage 1, ClO_4^- and SO_4^{2-} at Stage 2, and ClO_4^-, NO_3^-, and SO_4^{2-} simultaneously at Stage 3. The next stage only commenced when steady state of the current stage was reached in terms of effluent concentrations. ClO_4^-, NO_3^-, and SO_4^{2-} concentrations were selected to represent the typical levels in groundwater, with each being around 1 g m^{-3} (i.e., 0.36 g Cl m^{-3}), 10 g N m^{-3}, and 50 g m^{-3} (i.e., 16.7 g S m^{-3}), respectively. The DO concentration was constant at approximately 8 g m^{-3} at all three operating stages. Liquid samples were taken intensively and analysed for ClO_4^-, NO_2^-, NO_3^-, and SO_4^{2-} contents using ion chromatography (IC). Quantitative real-time polymerase chain reaction (qPCR) was used to monitor the microbial community in the biofilm. More details of configurations, operating tests, and analytical methods of the single-stage H_2-based MBfR can be found in Zhao et al. [19].

Experimental data from the two-stage H_2-based MBfR system reported in Zhao et al. [16] were used to validate the developed model. Two separate H_2-based MBfRs were connected in series, and both of the lead and lag MBfRs shared the similar configurations and inoculation process with the single-stage MBfR used for model calibration. After enrichment, two-phase tests with ClO_4^-, NO_3^-, SO_4^{2-}, and DO simultaneously but at different feeding rates were conducted with the two-stage MBfR system: 0.28 mL min^{-1} in Phase 1 and 0.42 mL min^{-1} in Phase 2. Phase 2 only commenced when steady state of Phase 1 was reached in terms of effluent concentrations. The feeding ClO_4^-, NO_3^-, SO_4^{2-}, and DO concentrations to the lead MBfR were set at 0.1 g m^{-3} (i.e., 0.036 g Cl m^{-3}), 6 g N m^{-3}, 22 g m^{-3} (i.e., 7.3 g S m^{-3}), and 8 g m^{-3}, respectively, during both phases. The effluent of the lead MBfR was

reoxygenated to around 8 g m^{-3} before it entered the lag MBfR. The H_2 pressure was kept at 17 psig in both MBfRs for all tests. Same methods applied to the MBfR for model calibration were used to analyse the liquid and biofilm samples taken from this two-stage H_2-based MBfR system. More details related to the two-stage H_2-based MBfR system configurations, operation, and analysis can be found in Zhao et al. [16].

2.3. Sensitivity analysis, model calibration, uncertainty analysis, and model validation

The poor agreement between the experimental data and the modeling results shown in Fig. S1 in the SI reveals the insufficiency of the model configured with parameters directly taken from reported literature to describe the H_2-based MBfR, especially in the simultaneous presence of ClO_4^-, NO_3^-, SO_4^{2-}, and DO in the feed. Therefore, a further model calibration is imperative to obtain a reliable model. In view of the considerable number of parameters involved in the model (see Table S4 in the SI), a sensitivity analysis was conducted using the AQUASIM built-in algorithms to locate the most important parameters of the developed model to describe the collective actions of HDB, PRB, SRB, SOB, and HB prior to the model calibration. The "absolute-relative" sensitivity function was used in this work, and the base values of parameters and initial conditions were set according to the literature reported values (see Table S4 in the SI) and the specific experimental settings of the single-stage MBfR used for model calibration. It should be noted that the yield of growth on H_2 and O_2 (i.e., Y_0) was obtained at 0.12 g COD g^{-1} COD by thermodynamic state calculations [27], which agreed with the reaction stoichiometry reported in Zhao et al. [19].

Model calibration based on experimental measurements of the single-stage H_2-based MBfR [19] was then only carried out for the most sensitive parameters through minimizing the sum of squares of the deviations between the experimental measurements and the model predictions, with the remaining parameters directly set as literature reported values.

Parameter estimation and uncertainty evaluation was conducted according to Batstone et al. [28] with a 95% confidence level for significance testing and parameter uncertainty analysis. A modified AQUASIM 2.1d was used to obtain the parameter surfaces [29].

Model validation was conducted with the calibrated model parameters using another independent experimental data sets reported for the two-stage H_2-based MBfR system [16]. The profiles of ClO_4^-, NO_3^-, and SO_4^{2-} for both the lead and lag MBfRs were used to assess the calibrated model.

2.4. Evaluating the effects of key operating conditions

The verified model was then applied to simulate the implementation of a single-stage H_2-based MBfR under different operating conditions, including influent ClO_4^- concentration, L_{H2}, HRT, and L_f. Altogether five different scenarios are considered in this work (shown in Table S5 in the SI). The first simulation scenario (i.e., Scenario 0 of Table S5) investigated the spatial distribution characteristics as well as the acting mechanisms behind the system performance through generating depth profiles of microbial community and substrates distribution and species-specific removal rates in the biofilm of the single-stage H_2-based MBfR. The ClO_4^-, NO_3^-, SO_4^{2-}, and DO concentrations for Scenario 0 were 0.18 g Cl m^{-3}, 10 g N m^{-3}, 10 g S m^{-3}, and 8 g m^{-3}, respectively. HRT, L_{H2}, and L_f were 3.67 h, 0.171 g COD m^{-2} h^{-1}, and 150 μm, respectively. As the ClO_4^- concentration in groundwater was normally much lower than NO_3^- and SO_4^{2-} and the effluent ClO_4^- concentration was found to be affected by the influent ClO_4^- loading [21], Scenario 1 of Table S5 was designed to unveil the effect of the influent ClO_4^- concentration on the single-stage H_2-based MBfR. The influent ClO_4^- concentration was varied from 0.036 to 0.36 g Cl m^{-3}, encompassing the concentrations used in the two H_2-based MBfR systems for model evaluation. Scenarios 2–4 of Table S5 explored the effects of L_{H2}, HRT, and L_f, respectively, on the steady-state reduction of ClO_4^-, NO_3^-, and SO_4^{2-} and the related microbial community structure of the single-stage MBfR. The combinations of operating conditions were chosen systematically over wide ranges of L_{H2} (0.074–0.195 g COD m^{-2} h^{-1}), HRT (1.33–4.67 h), and L_f (25–250 μm).

The initial concentrations of all soluble components in the biofilm and the bulk liquid for each simulation scenario were assumed to be zero. An average biofilm thickness was applied in the model without consideration of its variation with locations. All simulations assumed an initial biofilm thickness of 5 μm and were run for up to 500 days to reach steady-state conditions indicated by constant effluent concentrations, biofilm thickness, and microbial compositions in biofilm. The steady-state biofilm thickness was controlled by the surface detachment velocity equation reported in Ni and Yuan [30], and no re-attachment of detached particulates was considered in the model. The steady-state removal efficiencies of ClO_4^-, NO_3^-, and SO_4^{2-} and the H_2 utilization efficiency were used to evaluate the performance of the single-stage H_2-based MBfR.

3. Results and discussion

3.1. Sensitivity analysis

All the parameters of the developed model (see Table S4 in the SI) were assessed in the sensitivity analysis, with the effluent ClO_4^-, NO_3^-, and SO_4^{2-} concentrations of the single-stage MBfR at three operating stages being the model outputs. Fig. S2A–C in the SI indicate the sensitivities of the effluent ClO_4^-, SO_4^{2-}, and NO_3^- concentrations, respectively, to the top six most sensitive model parameters. Among all the parameters, the maximum growth rate in H_2-based denitrification (μ_1) and the maximum growth rate in H_2-based SO_4^{2-} reduction (μ_3) were found to exert the most determinant impacts on the effluent ClO_4^-, SO_4^{2-}, and NO_3^- concentrations simultaneously. Therefore, these two parameters could be reliably estimated in the model calibration process based on the experimental data from the single-stage MBfR reported in Zhao et al. [19].

3.2. Model calibration

μ_1 and μ_3 were estimated through fitting simulation results to the measured data obtained during the over 80-day operation of the single-stage MBfR. The best fit was obtained when μ_1 equalled 0.133 h^{-1} and μ_3 equalled 0.0062 h^{-1}. Fig. 1A illustrates the model predicted and measured dynamic profiles of ClO_4^-, SO_4^{2-}, and NO_3^- in the influent and effluent fluxes. At Stage 1 when SO_4^{2-} and NO_3^- were both absent, the ClO_4^- removal efficiency was close to 100%. When SO_4^{2-} was loaded initially at Stage 2, the SO_4^{2-} removal efficiency was low (around 10%), with most SO_4^{2-} leaving the MBfR with the effluent. However, the SO_4^{2-} removal efficiency increased to and stay about 78% after 6 days, owing to the increased activity of SRB. The addition of SO_4^{2-} in the influent didn't affect the complete ClO_4^- removal, with almost undetected ClO_4^- in the effluent. When NO_3^- (10 g N m^{-3}) was introduced at Stage 3, both the ClO_4^- and SO_4^{2-} removal was impacted due to the microbial competition for H_2. The ClO_4^- removal quickly dropped to as low as 20% but recovered to almost 100% after 3 days. Similarly, the SO_4^{2-} removal decreased to 24% firstly and then gradually recovered to around

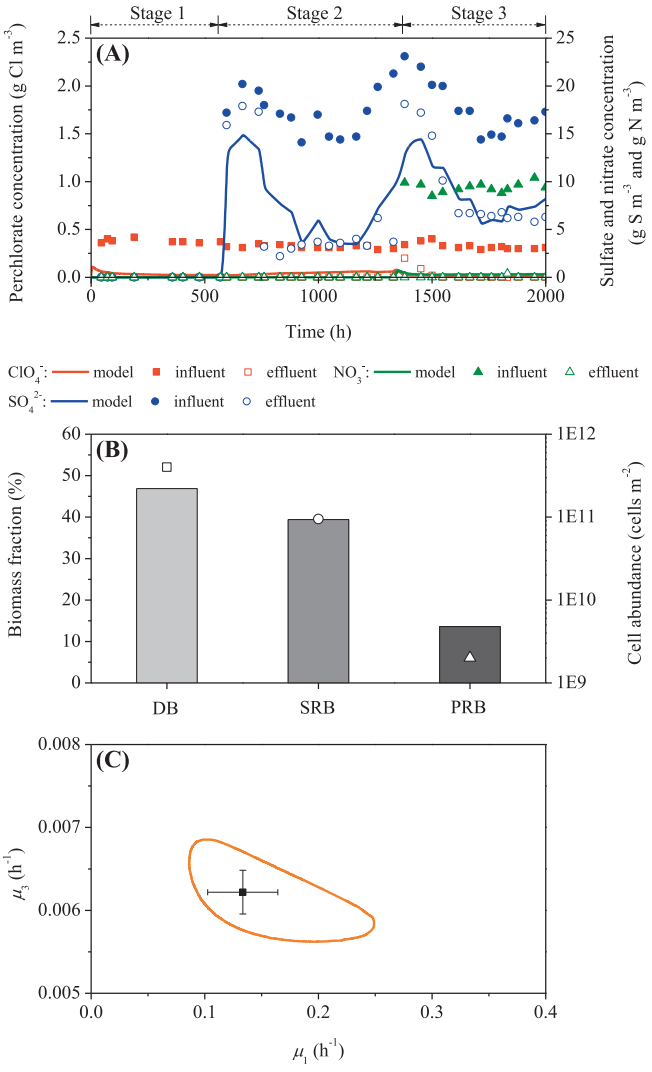

Fig. 1. Model calibration results based on the experimental data of the MBfR reported in Zhao et al. [19], fed with ClO_4^- at Stage 1, ClO_4^- and SO_4^{2-} at Stage 2, and ClO_4^-, SO_4^{2-} and NO_3^- simultaneously at Stage 3: (A) profiles of model predictions (lines) and experimental measurements (symbols) in terms of ClO_4^-, SO_4^{2-}, and NO_3^-; (B) model predicted biomass fraction in the biofilm (columns) and measured cell abundance of species (symbols) at Stage 3 (Only DB (i.e., HDB + HB), SRB, and PRB were considered with their total biomass fraction assumed as 100%); and (C) 95% confidence region for μ_1 and μ_3 as well as their best fits (in the centre) and standard errors obtained.

60% after 6 days. In contrast, the feeding NO_3^- was completely removed once it was introduced into the MBfR, with no NO_3^- as well as NO_2^- (data not shown) being detected in the effluent. In general, the model captured these variation trends well as shown in Fig. 1A. The model also predicted that the DO concentration in the effluent was below 0.15 g m^{-3} at all three stages, consistent with the assumption that oxygen was completely reduced in the MBfR made by Zhao et al. [19]. All these supported the validity of the calibrated model. Fig. 1B demonstrates the model predicted biomass fraction in the biofilm and the measured cell abundance of species using qPCR at steady state of Stage 3. Only denitrifying bacteria (DB, defined as the sum of HDB and HB in this work), SRB, and PRB were considered with their total biomass fraction assumed as 100%. According to the measured cell abundance, DB were the most abundant species coexisting with SRB in the biofilm and PRB were least abundant due to the relatively low ClO_4^- loading to the MBfR. The same trend was observed for the model predicted biomass fractions of these three main species as shown in Fig. 1B. This agreement further confirmed the validity of the developed model.

3.3. Uncertainty analysis

Fig. 1C shows the 95% confidence region for μ_1 and μ_3 together with their uncorrelated confidence intervals obtained during the model calibration process. The uncorrelated confidence intervals of both parameters were relatively small and fully covered by the correlated confidence region, which indicated a good level of reliability and identifiability of the estimated values. The calibrated value of μ_1 (0.133 h^{-1}) is higher than the value of 0.042 h^{-1} reported by Tang et al. [20]. μ_3 was calibrated to be 0.0062 h^{-1}, which is lower than the reported value of 0.0125 h^{-1} by Tang et al. [22]. The fact that the maximum growth rates in H_2-based denitrification (i.e., μ_1) and H_2-based ClO_4^- reduction (i.e., μ_2, with a value of 0.0625 h^{-1}) are higher than that in H_2-based SO_4^{2-} reduction (i.e., μ_3) indicates the competitive advantage of HDB and PRB over SRB for space in the biofilm when substrate availability is not a limiting factor. This kinetic feature could be utilized to favour the simultaneous removal of ClO_4^- and NO_3^- whilst restraining SO_4^{2-} reduction in the single-stage H_2-based MBfR.

3.4. Model validation

The validation of model and parameters was based on the comparison between the model predictions using the calibrated parameter values and another independent data sets reported for the two-stage H_2-based MBfR system. The model was first evaluated with the experimental data of the lead MBfR, with the model predictions and the experimental results shown in Fig. 2A. The increase of flow rate from 0.28 mL min^{-1} in Phase 1 to 0.42 mL min^{-1} in Phase 2 corresponded to an increase in the influent ClO_4^-, SO_4^{2-}, and NO_3^- loadings. As a result, the ClO_4^-, SO_4^{2-}, and NO_3^- removal all dropped from Phase 1 to Phase 2. As shown in Fig. 2A, the model predictions generally matched the measured data in terms of the effluent ClO_4^-, SO_4^{2-}, and NO_3^- concentrations during both phases. In addition, the model predicted biomass fractions in the biofilm captured the trend of the measured cell abundance of species of the lead MBfR at the end of Phase 1 as illustrated in Fig. 2B, which again supported the validity of the developed model.

Fig. 2C compares the model evaluation results with the experimental results of the lag MBfR. Different from the lead MBfR, the ClO_4^- and NO_3^- removal was complete in the lag MBfR during two running phases and was not compromised after flow rate elevation. A low SO_4^{2-} removal was observed in Phase 1. However, the increase of flow rate in Phase 2 avoided SO_4^{2-} reduction, thus reducing the SO_4^{2-} removal efficiency down to zero. Therefore, this two-stage MBfR system was effective in managing SO_4^{2-} reduction to a minimal level while achieving complete removal of ClO_4^- and NO_3^-. The good agreement between the model predictions and the measured data in terms of the effluent ClO_4^-, SO_4^{2-}, and NO_3^- concentrations during both phases strongly supported the validity of the developed model to describe the complicated competitive and cooperative interactions among microorganisms in H_2-based MBfRs fed with ClO_4^-, SO_4^{2-}, and NO_3^- simultaneously. The validity of the model was further verified by the acceptable match between the model predicted and measured trends in terms of microbial community structure in the biofilm of the lag MBfR at the end of Phase 1, as shown in Fig. 2D.

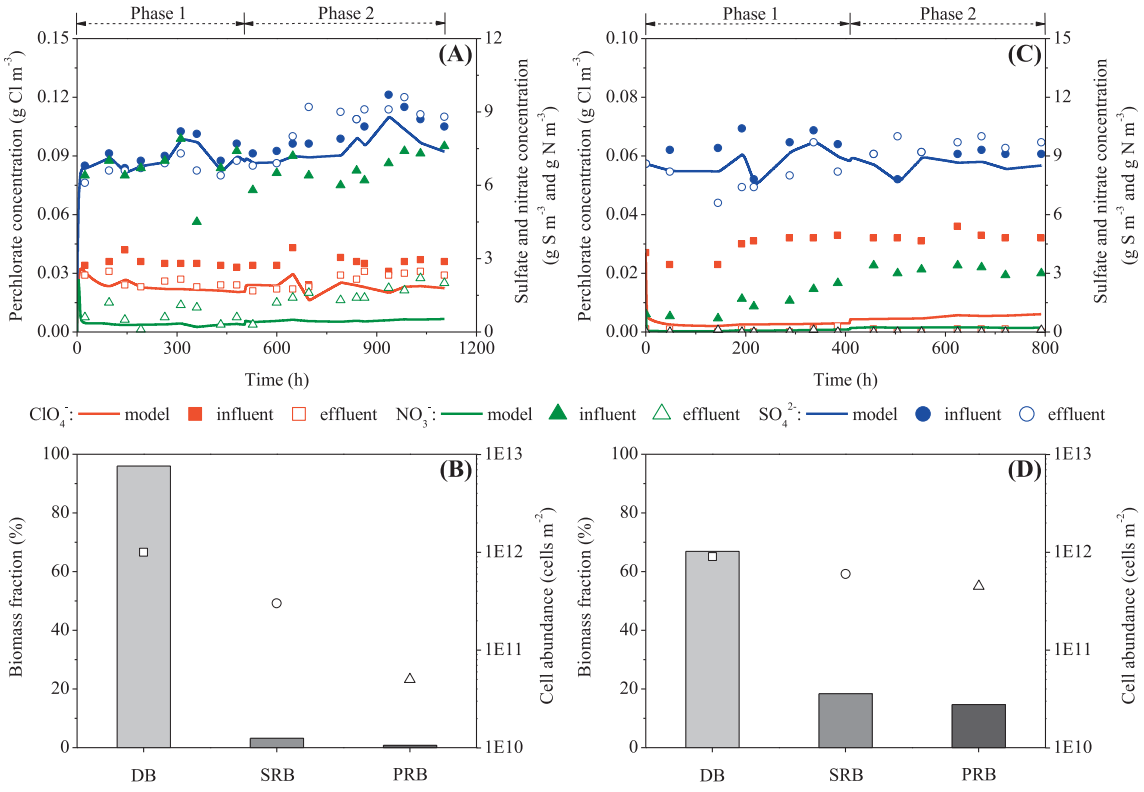

Fig. 2. Model validation results based on the experimental data of the (A and B) lead MBfR and (C and D) lag MBfR reported in Zhao et al. [16], with the influent feed rate controlled at 0.28 mL min^{-1} in Phase 1 and 0.42 mL min^{-1} in Phase 2: profiles of model predictions and experimental measurements of the (A) lead MBfR and (C) lag MBfR in terms of ClO_4^-, SO_4^{2-}, and NO_3^-; and model predicted biomass fraction in the biofilm (columns) and measured cell abundance of species (symbols) of the (B) lead MBfR and (D) lag MBfR at the end of Phase 1. Only DB (i.e., HDB + HB), SRB, and PRB were considered with their total biomass fraction assumed as 100%.

3.5. Characteristics in the biofilm of the single-stage H_2-based MBfR

Scenario 0 of Table S5 in the SI was used to investigate the spatial distribution in the biofilm and the acting mechanisms behind the system performance of the single-stage H_2-based MBfR treating ClO_4^-, SO_4^{2-}, and NO_3^- simultaneously. The steady-state ClO_4^-, SO_4^{2-}, and NO_3^- removal efficiencies were 86.2%, 80.9%, and 96.0%, respectively. The steady-state biomass distribution and substrates profiles as well as the species-specific removal rates of ClO_4^-, SO_4^{2-}, and NO_3^- within the biofilm under the operating conditions of Scenario 0 are shown in Fig. 3. As shown in Fig. 3A, HDB, PRB, and HB were mostly abundant (29%, 5%, and 21%, respectively) at the biofilm surface close to the bulk liquid where NO_3^- and ClO_4^- were supplied. However, the abundance of HDB, PRB, and HB gradually decreased to 9%, 2%, and 1%, respectively, at the base of the biofilm. This trend was opposite to the simulation results by Tang et al. [20], which was mainly due to the additional microbial competition of SRB. The abundance of SRB was 41% at the base of the biofilm where H_2 was provided but decreased to 5% at the biofilm surface, similar to the simulation trend observed for the high H_2 supply case by Tang et al. [22]. SOB were washed out and not present over the entire biofilm range. EPS were prevalent across the whole biofilm with the abundance of around 40%. Inert organics produced from biomass decay were higher on the membrane side, with the abundance slightly decreasing from 6% to 2% (Fig. 3A).

The associated substrate profiles within the biofilm are shown in Fig. 3B. The ClO_4^-, SO_4^{2-}, and NO_3^- concentrations all decreased from the bulk liquid where they were provided to the base of the biofilm. However, NO_3^- showed a higher decreasing rate due to its consumption by HDB, HB, and PRB simultaneously. In contrast, H_2 decreased from the membrane surface where it was supplied towards the bulk liquid. The trend was same with the distribution profile of SRB (shown in Fig. 3A), implying the dependence of SRB growth on the H_2 supply in the presence of competitors such as HDB and PRB. The produced SMP gradually diffused into the bulk liquid, thus rending a higher concentration on the membrane side. DO was quickly consumed within the top biofilm layer, while the S^{2-} concentration stayed almost unchanged across the biofilm due to the absence of SOB under the simulation conditions of Scenario 0.

The counter-diffusional supply of gas and liquid substrates resulted in the stratified microbial community structure and hence the activity stratification in the biofilm of the single-stage H_2-based MBfR, as evidenced by the simulated removal rates of ClO_4^-, SO_4^{2-}, and NO_3^- in the biofilm under the operating conditions of Scenario 0 shown in Fig. 3C. The ClO_4^- and NO_3^- removal mainly occurred in the outer layer of the biofilm, while the SO_4^{2-} reduction mostly took place in the inner layer of the biofilm. This spatial distribution of species-specific activities was commensurate with the microbial distribution profiles in Fig. 3A. Under the given operating conditions of Scenario 0, SRB and PRB were fully responsible for the SO_4^{2-} and ClO_4^- removal, respectively, while HDB, PRB, and HB each accounted for approximately 77%, 13%, and 10% of the NO_3^- removed, respectively. This heterogeneous, stratified characteristic of biofilm in the single-stage H_2-based MBfR was controlled by operating conditions and therefore opened the operational window for minimizing SO_4^{2-} reduction without hindering ClO_4^- and NO_3^- removal through the implementation of selection pressure, which was explored in the next section.

3.6. Key factors affecting the single-stage H_2-based MBfR

The impact of the influent ClO_4^- concentration on the steady-state system performance (including the reduction of ClO_4^-, NO_3^-,

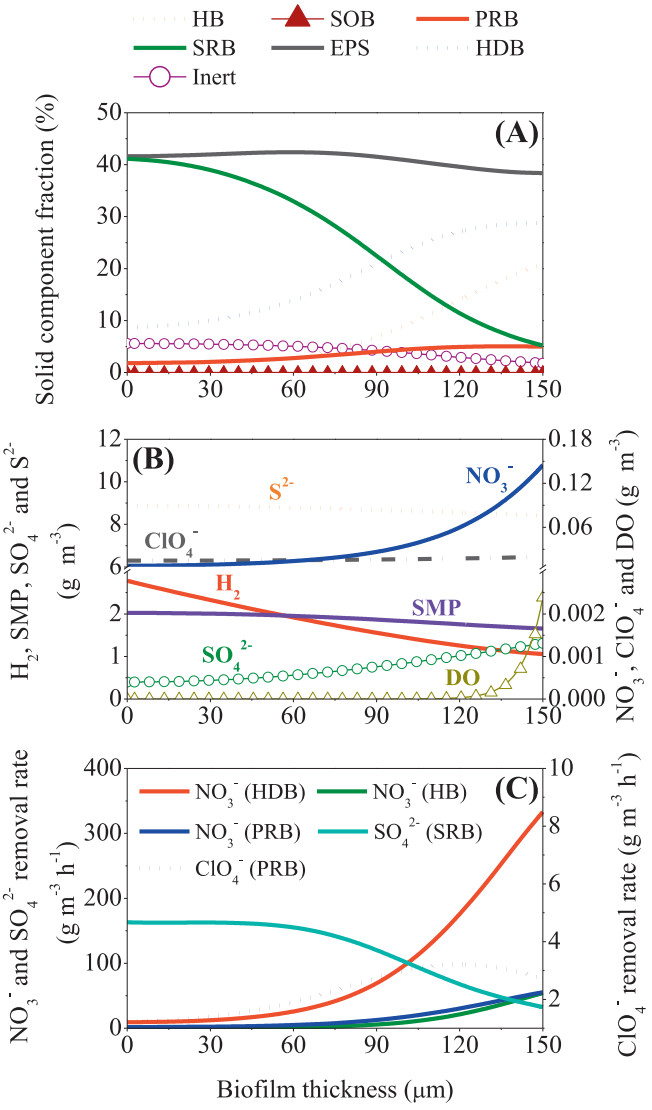

Fig. 3. Model simulation results of the MBfR with ClO_4^-, NO_3^-, and SO_4^{2-} simultaneously in the influent based on Scenario 0 in Table S5 (depth zero represents the membrane surface): (A) distribution profiles of solid species; (B) distribution profiles of dissolved species; and (C) species-specific removal rates of ClO_4^-, NO_3^-, and SO_4^{2-}.

and SO_4^{2-} as well as the H_2 utilization) and microbial community structure of the single-stage H_2-based MBfR (Scenario 1 of Table S5) is shown in Fig. 4A. The ClO_4^- removal efficiency was only 55.8% at the influent ClO_4^- concentration of 0.036 g Cl m^{-3}, but gradually increased with the increasing ClO_4^- concentration in the influent and reached 90.2% at the influent ClO_4^- concentration of 0.36 g Cl m^{-3}. On the contrary, the corresponding SO_4^{2-} removal efficiency slightly decreased from 81.0% to 80.6%. The NO_3^- removal efficiency was not affected by the influent ClO_4^- concentration, which was consistent with Tang et al. [21] and Nerenberg et al. [15], and was stable at 96.0%. The H_2 utilization efficiency was also stable at 98.9% over the range of the influent ClO_4^- concentration studied. The changing microbial community structure in the biofilm under different influent ClO_4^- concentration conditions contributed to the varying system performance, as delineated in Fig. 4A. At the low influent ClO_4^- concentration of 0.036 g Cl m^{-3}, HDB, HB, and SRB dominated the biofilm, while the fraction of PRB was only 1%. With the increasing influent ClO_4^- concentration, PRB gained advantage in competing with SRB and HDB for H_2 and hence with HDB for NO_3^-. As a result, the fraction of PRB increased while those of SRB and HDB decreased. However, the combined biomass fraction of PRB and HDB maintained about 40% in the biofilm, leading to the almost unchanged NO_3^- removal efficiency in Fig. 4A. The fraction of HB stayed around 14% while that of SOB remained null over the range studied. Though found to be proportional to the steady-state ClO_4^- removal, the influent ClO_4^- concentration only exerted a lesser role in affecting the SO_4^{2-} removal under the simulation conditions of Scenario 1.

The relationship between the H_2 surface loading and the steady-state system performance as well as microbial community structure of the single-stage H_2-based MBfR (Scenario 2 of Table S5) is shown in Fig. 4B. When L_{H2} was relatively low (<0.103 g COD m^{-2} h^{-1}), HDB dominated the biofilm with the coexistence of a low fraction of HB (<11%), due to their competitive advantage over SRB and PRB for H_2. As a consequence, the H_2 supplied was completely consumed. The removal efficiencies of ClO_4^- and SO_4^{2-} were both zero while the NO_3^- removal efficiency kept increasing from 54.4% at L_{H2} of 0.074 g COD m^{-2} h^{-1}. The increase of L_{H2} to 0.114 g COD m^{-2} h^{-1} increased the availability of H_2 for PRB. Consequently, PRB (11%) appeared and coexisted with HDB (84%) and HB (5%) in the biofilm, rendering the ClO_4^- and NO_3^- removal efficiencies of 82.7% and 91.9%, respectively, at L_{H2} of 0.114 g COD m^{-2} h^{-1}. Further increase in L_{H2} stimulated the growth and enhanced the fraction of SRB but depressed those of HDB and PRB, giving rise to emerging SO_4^{2-} removal efficiency of 18.6% at L_{H2} of 0.126 g COD m^{-2} h^{-1} and the ever-increasing SO_4^{2-} removal thereafter. However, excessive H_2 supply of over 0.171 g COD m^{-2} h^{-1} wouldn't make further significant change to the microbial community structure, with HDB, PRB, SRB, and HB taking up 33%, 6%, 47%, and 14% of the total active biomass, respectively. The resulting ClO_4^-, SO_4^{2-}, and NO_3^- removal efficiencies maintained at 86.3%, 81.1%, and 96.1%, respectively. The accompanying H_2 utilization efficiency dropped consistently from 100% to 86.3% at L_{H2} of 0.195 g COD m^{-2} h^{-1}. Over the range of L_{H2} studied, SOB didn't grow in the biofilm mainly due to either their loss in competing for oxygen or the unavailability of sulfide produced. These findings demonstrated the importance of H_2 supply as a control strategy in operating this single-stage H_2-based MBfR. As shown in Fig. 4B, a too low L_{H2} would suppress the SO_4^{2-} reduction but compromise the removal of ClO_4^- and NO_3^-, while a too high L_{H2} not only meant energy wastage but also triggered the SO_4^{2-} reduction which agreed with the findings of Martin et al. [31]. Under the operating conditions of Scenario 2, a L_{H2} of around 0.114 g COD m^{-2} h^{-1} could be considered most suitable.

The dependence of the steady-state microbial community structure and system performance of the single-stage H_2-based MBfR on HRT (Scenario 3 of Table S5) is depicted in Fig. 4C. An HRT of lower than 2 h provided sufficient electron acceptors and therefore intensified the competitions between HDB, PRB, and SRB for the electron donor (i.e., H_2), resulting in the dominance of HDB and HB in the biofilm. Hence, the NO_3^- removal efficiency increased with the increasing HRT. Albeit the H_2 supplied was completely used, neither ClO_4^- nor SO_4^{2-} was removed. However, PRB emerged in the biofilm and accounted for 14% of the total active biomass when the HRT increased to 2.33 h. A proportion of H_2 was shunted to the respiration of PRB, leading to the sudden increase of the ClO_4^- removal efficiency to 79.4% at HRT of 2.33 h. The corresponding NO_3^- removal efficiency also increased to 88.9% owing to the additional contribution from PRB. Further increase in HRT favoured the growth of SRB. Consequently, the fraction of SRB and the SO_4^{2-} removal efficiency after the first appearance at HRT of 2.33 h showed a steadily increasing trend, reaching 54% and 86.1% at HRT of 4.67 h, respectively. This was similar to the simulation trend obtained in the single-stage H_2-based MBfR fed with SO_4^{2-} and NO_3^- (but no ClO_4^-) by

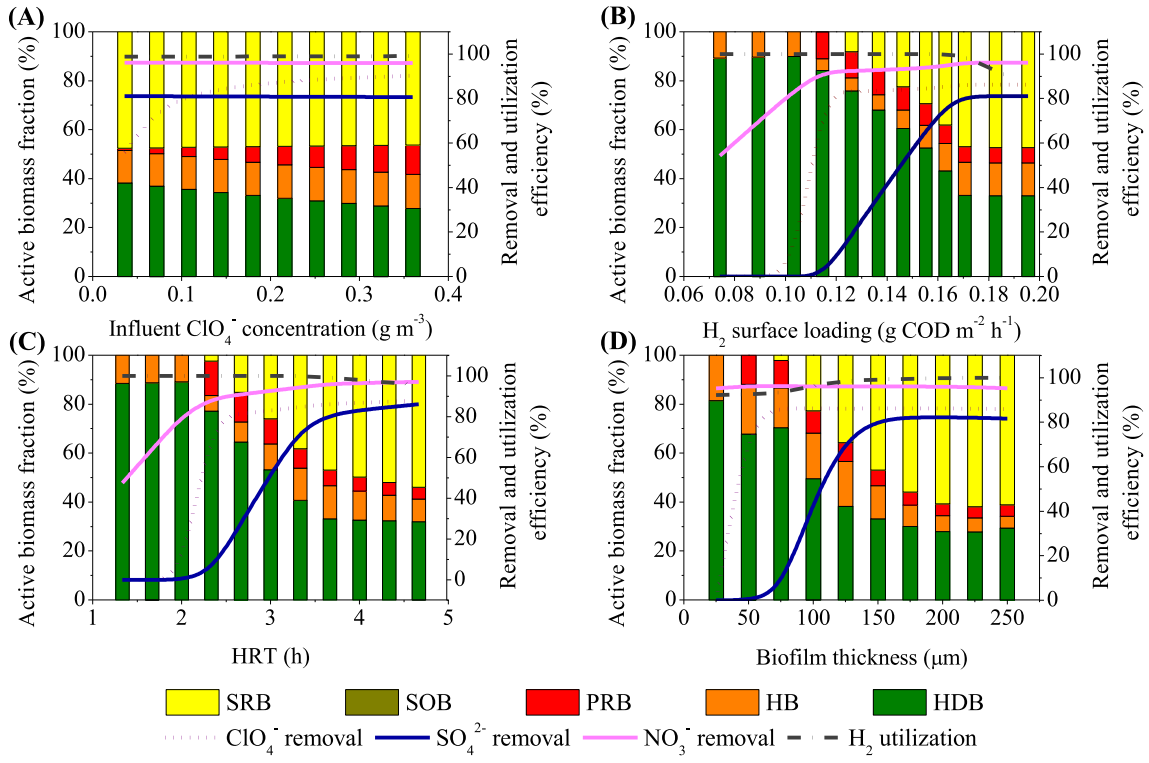

Fig. 4. Model simulation results of the MBfR with ClO_4^-, NO_3^-, and SO_4^{2-} simultaneously in the influent from Scenarios 1 to 4 in Table S5: (A) effect of influent ClO_4^- concentration; (B) effect of H_2 surface loading; (C) effect of HRT; and (D) effect of biofilm thickness on the ClO_4^-, SO_4^{2-}, and NO_3^- removal efficiencies, H_2 utilization efficiency, and microbial community structure in the biofilm.

Tang et al. [22]. Though the corresponding fractions of HDB and PRB decreased and approached 32% and 5% at HRT of 4.67 h, the ClO_4^- and NO_3^- removal efficiencies slightly increased and remained above 85.0% and 94.0%, respectively. A high HRT meant a low influent loading of electron acceptors, corresponding to a relatively high loading of electron donor (i.e., H_2) under the simulation conditions of Scenario 3. This was also reflected by the decreasing H_2 utilization efficiency when HRT exceeded 3.67 h, as shown in Fig. 4C. SOB were absent from the biofilm within the range of HRT studied. Therefore, HRT should also be properly managed at a certain value (e.g., about 2.33 h under the operating conditions of Scenario 3) to maximize the removal of ClO_4^- and NO_3 whilst minimizing the SO_4^{2-} reduction.

Fig. 4D illustrates the impact of biofilm thickness on the steady-state system performance and microbial community structure of the single-stage H_2-based MBfR (Scenario 4 of Table S5). The ClO_4^- removal efficiency was zero at L_f of 25 μm but quickly increased to 82.1% at L_f of 50 μm and kept above 85.0% at L_f of more than 75 μm. There was no SO_4^{2-} removal until L_f reached 75 μm with a removal efficiency of 3.4%. Further increasing in L_f favoured the SO_4^{2-} removal, with the efficiency increasing to 81.6% at L_f of 250 μm. An increasing trend was also observed for the H_2 utilization efficiency, which increased from 92.2% at L_f of 25 μm to 100.0% at L_f of 250 μm. The NO_3^- removal efficiency was not subject to significant change over the L_f range studied and stayed above 95.0%. Biofilm thickness therefore should be properly controlled in the single-stage MBfR.

Overall, a thin biofilm (e.g., L_f of 50 and 75 μm in this case) was beneficial for the high-level simultaneous removal of ClO_4^- and NO_3^- through supporting the coexistence of HDB, PRB, and HB in the biofilm, as shown in Fig. 4D. In contrast, a thick biofilm (e.g., L_f of more than 100 μm in this case) provided favourable environment and protected space (i.e., inner layer of the biofilm) for SRB, stimulated their growth [31], and therefore compromised the biomass fractions of HDB and PRB in the biofilm, resulting in the increasing SO_4^{2-} reduction. Moreover, the process optimization of the H_2-based MBfR in consideration of various operating conditions explored in this work is feasible via modeling but warrants further work.

Although the model was only tested using lab-scale experimental data and future experimental verification of the results is needed, the main objective of this work was to develop, calibrate, validate, and apply a multi-species biofilm model for qualitatively and quantitatively assessing the single-stage H_2-based MBfR with multiple microbial species, feeding substrates, and acting mechanisms involved, in order to provide a clear picture in terms of impacts of key operating conditions on the reduction of ClO_4^-, NO_3^-, and SO_4^{2-} of the single-stage H_2-based MBfR to facilitate its practical application. In this sense, the simulation results obtained still provide useful information for the potential pilot-scale or even full-scale design and operation/optimization of the H_2-based MBfR treating ClO_4^-, NO_3^-, and SO_4^{2-} simultaneously.

4. Conclusions

A biofilm model integrating the key mechanisms of microbially-mediated ClO_4^-, NO_3^-, and SO_4^{2-} reduction in the H_2-based MBfR was calibrated and validated using the experimental data of reported H_2-based MBfRs. The model was then applied to evaluate the effects of key operating conditions on the single-stage H_2-based MBfR. The results show that the steady-state reduction of ClO_4^-, NO_3^-, and SO_4^{2-} and the microbial community structure in the single-stage H_2-based MBfR was highly dependent on the influent ClO_4^- concentration, H_2 surface loading, HRT, and biofilm thickness. A higher influent ClO_4^- concentration led to a higher ClO_4^- removal

efficiency, compensated by a slightly decreasing SO_4^{2-} removal. The H_2 loading should be properly managed at certain critical level to maximize the ClO_4^- and NO_3^- removal while limiting the growth of SRB which would occur in the case of excessive H_2 supply. A moderate HRT and a relatively thin biofilm were required to maintain high-level removal of ClO_4^- and NO_3^- but restrict the SO_4^{2-} reduction. The developed model offers a useful and powerful tool to facilitate the design of such a single-stage H_2-based MBfR, and the simulation results of this work provide important control strategies to effectively achieve high-level simultaneous removal of ClO_4^- and NO_3^- whilst avoiding the unwanted SO_4^{2-} reduction.

Acknowledgements

This study was supported by Australian Research Council (ARC) through Project DP130103147. Xueming Chen acknowledges China Scholarship Council (CSC) for the scholarship support. Bing-Jie Ni acknowledges the support of ARC Future Fellowship (FT160100195) and The University of Queensland Fellowship.

Appendix A. Supplementary data

Supplementary data associated with this article can be found, in the online version, at http://dx.doi.org/10.1016/j.cej.2017.01.084.

References

[1] K.H. Kucharzyk, R.L. Crawford, B. Cosens, T.F. Hess, Development of drinking water standards for perchlorate in the United States, J. Environ. Manage. 91 (2009) 303–310.
[2] B.E. Logan, Assessing the outlook for perchlorate remediation, Environ. Sci. Technol. 35 (2001) 482a–487a.
[3] J.D. Coates, L.A. Achenbach, Microbial perchlorate reduction: rocket-fuelled metabolism, Nat. Rev. Microbiol. 2 (2004) 569–580.
[4] Y.H. Luo, R. Chen, L.L. Wen, F. Meng, Y. Zhang, C.Y. Lai, B.E. Rittmann, H.P. Zhao, P. Zheng, Complete perchlorate reduction using methane as the sole electron donor and carbon source, Environ. Sci. Technol. 49 (2015) 2341–2349.
[5] B. Gu, J.D. Coates, Perchlorate: Environmental Occurrence, Interactions and Treatment, Springer Science & Business Media, 2006.
[6] L. Knobeloch, B. Salna, A. Hogan, J. Postle, H. Anderson, Blue babies and nitrate-contaminated well water, Environ. Health Perspect. 108 (2000) 675–678.
[7] D. Chen, K. Yang, H.Y. Wang, B. Lv, Nitrate removal from groundwater by hydrogen-fed autotrophic denitrification in a bio-ceramsite reactor, Water Sci. Technol. 69 (2014) 2417–2422.
[8] I. Zhu, T. Getting, A review of nitrate reduction using inorganic materials, Environ. Technol. Rev. 1 (2012) 46–58.
[9] H.P. Zhao, S. Van Ginkel, Y.N. Tang, D.W. Kang, B. Rittmann, R. Krajmalnik-Brown, Interactions between perchlorate and nitrate reductions in the biofilm of a hydrogen-based membrane biofilm reactor, Environ. Sci. Technol. 45 (2011) 10155–10162.
[10] B.E. Rittmann, R. Nerenberg, K.C. Lee, I. Najm, T.E. Gillogly, G.E. Lehman, S.S. Adham, Hydrogen-based hollow-fiber membrane biofilm reactor (MBfR) for removing oxidized contaminants, Water Sci. Technol. 4 (2004) 127–133.
[11] M. Ziv-El, S.C. Popat, K. Cai, R.U. Halden, R. Krajmalnik-Brown, B.E. Rittmann, Managing methanogens and homoacetogens to promote reductive dechlorination of trichloroethene with direct delivery of H_2 in a membrane biofilm reactor, Biotechnol. Bioeng. 109 (2012) 2200–2210.
[12] L.S. Downing, R. Nerenberg, Kinetics of microbial bromate reduction in a hydrogen-oxidizing, denitrifying biofilm reactor, Biotechnol. Bioeng. 98 (2007) 543–550.
[13] C.Y. Lai, X.E. Yang, Y.N. Tang, B.E. Rittmann, H.P. Zhao, Nitrate shaped the selenate-reducing microbial community in a hydrogen-based biofilm reactor, Environ. Sci. Technol. 48 (2014) 3395–3402.
[14] K.C. Lee, B.E. Rittmann, Applying a novel autohydrogenotrophic hollow-fiber membrane biofilm reactor for denitrification of drinking water, Water Res. 36 (2002) 2040–2052.
[15] R. Nerenberg, B.E. Rittmann, I. Najm, Perchlorate reduction in a hydrogen-based membrane-biofilm reactor, J. Am. Water Works Assoc. 94 (2002) 103–114.
[16] H.-P. Zhao, A. Ontiveros-Valencia, Y. Tang, B.O. Kim, Z.E. Ilhan, R. Krajmalnik-Brown, B. Rittmann, Using a two-stage hydrogen-based membrane biofilm reactor (MBfR) to achieve complete perchlorate reduction in the presence of nitrate and sulfate, Environ. Sci. Technol. 47 (2013) 1565–1572.
[17] I. Pikaar, K.R. Sharma, S.H. Hu, W. Gernjak, J. Keller, Z.G. Yuan, Reducing sewer corrosion through integrated urban water management, Science 345 (2014) 812–814.
[18] Y. Chen, J.J. Cheng, K.S. Creamer, Inhibition of anaerobic digestion process: a review, Bioresour. Technol. 99 (2008) 4044–4064.
[19] H.-P. Zhao, Z.E. Ilhan, A. Ontiveros-Valencia, Y. Tang, B.E. Rittmann, R. Krajmalnik-Brown, Effects of multiple electron acceptors on microbial interactions in a hydrogen-based biofilm, Environ. Sci. Technol. 47 (2013) 7396–7403.
[20] Y. Tang, H. Zhao, A.K. Marcus, R. Krajmalnik-Brown, B.E. Rittmann, A steady-state biofilm model for simultaneous reduction of nitrate and perchlorate, part 1: model development and numerical solution, Environ. Sci. Technol. 46 (2012) 1598–1607.
[21] Y.N. Tang, H.P. Zhao, A.K. Marcus, R. Krajmalnik-Brown, E.R. Bruce, A steady-state biofilm model for simultaneous reduction of nitrate and perchlorate, part 2: parameter optimization and results and discussion, Environ. Sci. Technol. 46 (2012) 1608–1615.
[22] Y. Tang, A. Ontiveros-Valencia, L. Feng, C. Zhou, R. Krajmalnik-Brown, B.E. Rittmann, A biofilm model to understand the onset of sulfate reduction in denitrifying membrane biofilm reactors, Biotechnol. Bioeng. 110 (2013) 763–772.
[23] P. Reichert, AQUASIM 2.0-Computer Program for the Identification and Simulation of Aquatic Systems, EAWAG, Dubendorf, Switzerland, 1998.
[24] A. Terada, S. Lackner, S. Tsuneda, B.F. Smets, Redox-stratification controlled biofilm (ReSCoBi) for completely autotrophic nitrogen removal: the effect of co- versus counter-diffusion on reactor performance, Biotechnol. Bioeng. 97 (2007) 40–51.
[25] X. Chen, J. Guo, Y. Shi, S. Hu, Z. Yuan, B.-J. Ni, Modeling of simultaneous anaerobic methane and ammonium oxidation in a membrane biofilm reactor, Environ. Sci. Technol. 48 (2014) 9540–9547.
[26] X. Chen, J. Guo, G.-J. Xie, Y. Liu, Z. Yuan, B.-J. Ni, A new approach to simultaneous ammonium and dissolved methane removal from anaerobic digestion liquor: a model-based investigation of feasibility, Water Res. 85 (2015) 295–303.
[27] R. Kleerebezem, M.C.M. Van Loosdrecht, A generalized method for thermodynamic state analysis of environmental systems, Crit. Rev. Environ. Sci. Technol. 40 (2010) 1–54.
[28] D.J. Batstone, P.F. Pind, I. Angelidaki, Kinetics of thermophilic, anaerobic oxidation of straight and branched chain butyrate and valerate, Biotechnol. Bioeng. 84 (2003) 195–204.
[29] H. Ge, P.D. Jensen, D.J. Batstone, Pre-treatment mechanisms during thermophilic–mesophilic temperature phased anaerobic digestion of primary sludge, Water Res. 44 (2010) 123–130.
[30] B.J. Ni, Z.G. Yuan, A model-based assessment of nitric oxide and nitrous oxide production in membrane-aerated autotrophic nitrogen removal biofilm systems, J. Membr. Sci. 428 (2013) 163–171.
[31] K.J. Martin, C. Picioreanu, R. Nerenberg, Assessing microbial competition in a hydrogen-based membrane biofilm reactor (MBfR) using multidimensional modeling, Biotechnol. Bioeng. 112 (2015) 1843–1853.